Title
Analysis of surface-tension-driven blood flow using spectral domain optical coherence tomography

ISBN
978-0-8194-7061-4

Authors
Ahn, Yeh-Chan
Cito, Salvatore
Katakis, Ioanis
et al.

Publication Date
2008-02-07

DOI
10.1117/12.764709

Analysis of surface-tension-driven blood flow using spectral domain optical coherence tomography

Yeh-Chan Ahn*[a], Salvatore Cito[a,b], Ioanis Katakis[b], Jordi Pallares[c], Zhongping Chen[a]

[a]Beckman Laser Institute and Department of Biomedical Engineering, University of California, Irvine, 1002 Health Sciences Rd. E., Irvine, CA, USA 92617; [b]Department of Chemical Engineering, Universitat Rovira i Virgili, Tarragona, Spain, [c]Department of Mechanical Engineering, Universitat Rovira i Virgili, Tarragona, Spain

ABSTRACT

Passive pumping for lab-on-a-chip using surface tension only is the most effective method because the effect of surface tension on flow is significant in microscale. The movement of the triple point at a meniscus is driven by surface tension, resisted by viscous stress, and balanced by inertial force. In previous studies, the meniscus motion has been predicted theoretically with a one-dimensional model. However, three-dimensional flow field around the meniscus and the effect of cross-sectional shapes on the flow have not yet been assessed. Here, we visualized and analyzed the surface-tension-driven blood flow using spectral-domain Doppler optical coherence tomography.

Keywords: Surface-tension-driven flow, blood flow, optical coherence tomography, radial velocity, mass transfer enhancement

1. INTRODUCTION

Microfluidics emerged in the beginning of the 1980s and is used in the development of inkjet printheads, DNA chips, lab-on-a-chip technology, micro-propulsion, and micro-thermal technologies. The advent of microfluidic devices has brought people a need for better understanding of the flows in capillary microchannels. In order to induce the flows in the microchannels, conventional pressure-driven methods are inadequate because they require an active pumping mechanism and turn out to have a high pumping pressure. Novel passive pumping mechanisms that take advantage of high surface–volume ratio have been tried, including the surface-tension-driven method, droplet and bubble based thermocapillary, viscosity-temperature dependent valveless micropump, electroosmosis, electrowetting, electrohydrodynamic effect etc. Among them, the surface-tension-driven method is suitable for handheld, disposable, and on-site diagnostic applications which usually utilize biological liquids like blood.

When the microchannel comes in contact with a blood droplet, surface tension draws it into the microchannel and sets the blood into motion. At the common line of intersection of the blood–gas interface and the solid wall of the microchannel, the three surface tension forces originating from blood-gas, blood-solid, and gas-solid interactions stay in local equilibrium by establishing a certain contact angle. Maintenance of this state of equilibrium pulls the blood toward the meniscus bounded by the common line which moves along the blood motion as well. It, however, is not a straightforward way to determine the surface tension forces or the contact angle in this situation with a moving common line. The contact angle would rather evolve dynamically due to the interrelation between the surface tension forces and the meniscus speed.

Pioneering attempts to understand the surface-tension-driven flows for practical applications have been made by Lucas[1] and Washburn.[2] By assuming a steady-state flow, they obtained a solution for the, so-called, Lucas–Washburn equation. The solution states that the meniscus position is governed by the square root of time. In the literature, there have been several decades of research reporting on the dynamics of the meniscus, wetting and spreading as well as reconciling of the no-slip condition of the common line motion.[3-7] Further, there have been many theoretical and experimental studies on surface-tension-driven flows.[8-14] Recently, Chakraborty[15] studied theoretically the effect of suspended erythrocytes on non-Newtonian flow characteristics and the implication of the dynamically-evolving contact angle. These studies,

Microfluidics, BioMEMS, and Medical Microsystems VI, edited by Wanjun Wang, Claude Vauchier,
Proc. of SPIE Vol. 6886, 68860S, (2008) · 0277-786X/08/$18 · doi: 10.1117/12.764709

however, are one-dimensional models which focus on the meniscus speed but cannot account for the radial liquid velocity, particularly in the surface traction regime near the meniscus.

In order to explore and quantify biochemical reactions, such as DNA hybridization and antigen-antibody binding, it is important to know the radial velocity. The radial velocity enhances mass transfer over reactive surfaces in the microchannels. For instance, the surface plasmon resonance sensor, which is a surface-based detection system to monitor adsorption of biological molecules onto the surface of a gold film, can get a high sample capture fraction and minimize sample consumption by radial velocity.

In this study, we assessed the axial and the radial velocity field of the surface-tension-driven blood flow with spectral-domain Doppler optical coherence tomography (SDDOCT). SDDOCT is an emerging imaging modality that has high-speed, high-resolution, non-invasive, cross-sectional imaging capability through turbid biofluids. Since SDDOCT allows simultaneous real-time visualization of sample structure and flow, it is often compared to clinical ultrasound. However, the spatial resolution of clinical ultrasound is limited to approximately 100 μm due to the relatively long wavelength of acoustic waves. SDDOCT takes advantage of the short coherence length of broadband light sources in order to achieve cross-sectional images with micrometer (2–10 μm) scale resolution. SDDOCT is also superior to ultrasound in that SDDOCT is operated in non-contact-mode. Because of the aforementioned merits, SDDOCT is receiving a great deal of attention in the area of microscale flow visualization.[16]

2. EXPERIMENTAL SETUP

The schematic of SDDOCT is shown in Fig. 1. Low-coherence light having a 1310 nm center wavelength with a full width at half maximum of 95 nm was coupled into the source arm of a fiber-based Michelson interferometer. Backscattered lights from the reference and sample arms were guided into a spectrometer. Interference fringes were sampled by the spectrometer with a 1×1024 InGaAs detector array at 7.7 kHz. The wavelength range on the array was 130 nm, corresponding to a spectral resolution of 0.13 nm and an imaging depth (from *A* to *A*') of 3.4 mm in air. The probe beam with a 15 μm spot at the focal point was fixed at the center of the microchannel. The microchannel was tilted by 2^{o} from the horizon using an accurate goniometer to avoid possible detector saturation by a strong backscattering from the microchannel surface. This angle sets the Doppler angle between the backscattered light and the velocity of blood cells. We used microchannels with different sizes and cross-sectional shapes: three circular microchannels with inner diameters of 300 μm, 400 μm, and 500 μm, and two square microchannels with widths of 300 μm and 500 μm. A method to get the sample structure and velocity from the interference fringes was well described in the authors' previous paper.[16]

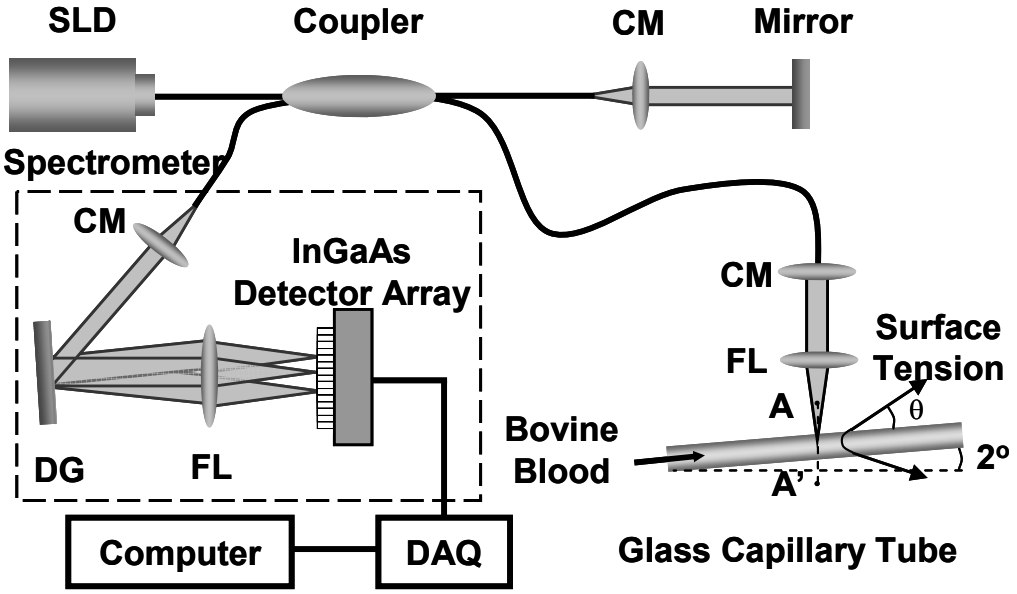

Fig. 1. Schemetic diagram for spectral-domain Doppler optical coherence tomography. SLD: Superluminescent Diode; CM: collimator; DG: diffraction grating; FL: focusing lens.

3. EXPERIMENTAL RESULTS

From a video analysis, we first measured the meniscus position over time for the different microchannels and computed the meniscus speed for each position as shown in Fig. 2. Elapsed time for the meniscus to reach a position was obtained by averaging three ensemble sets. Then we fitted the meniscus position data from the circular microchannels with the Lucas–Washburn one-dimensional model, Eq. (1), and found the best fit with $\Gamma\cos\theta/\mu$=8.46 within the range (200 μm – 500 μm) of inner diameter. The solution of the Lucas–Washburn equation for a circular microchannel can be obtained as:

$$h = \sqrt{\frac{a\Gamma\cos\theta}{2\mu}t}\,, \tag{1}$$

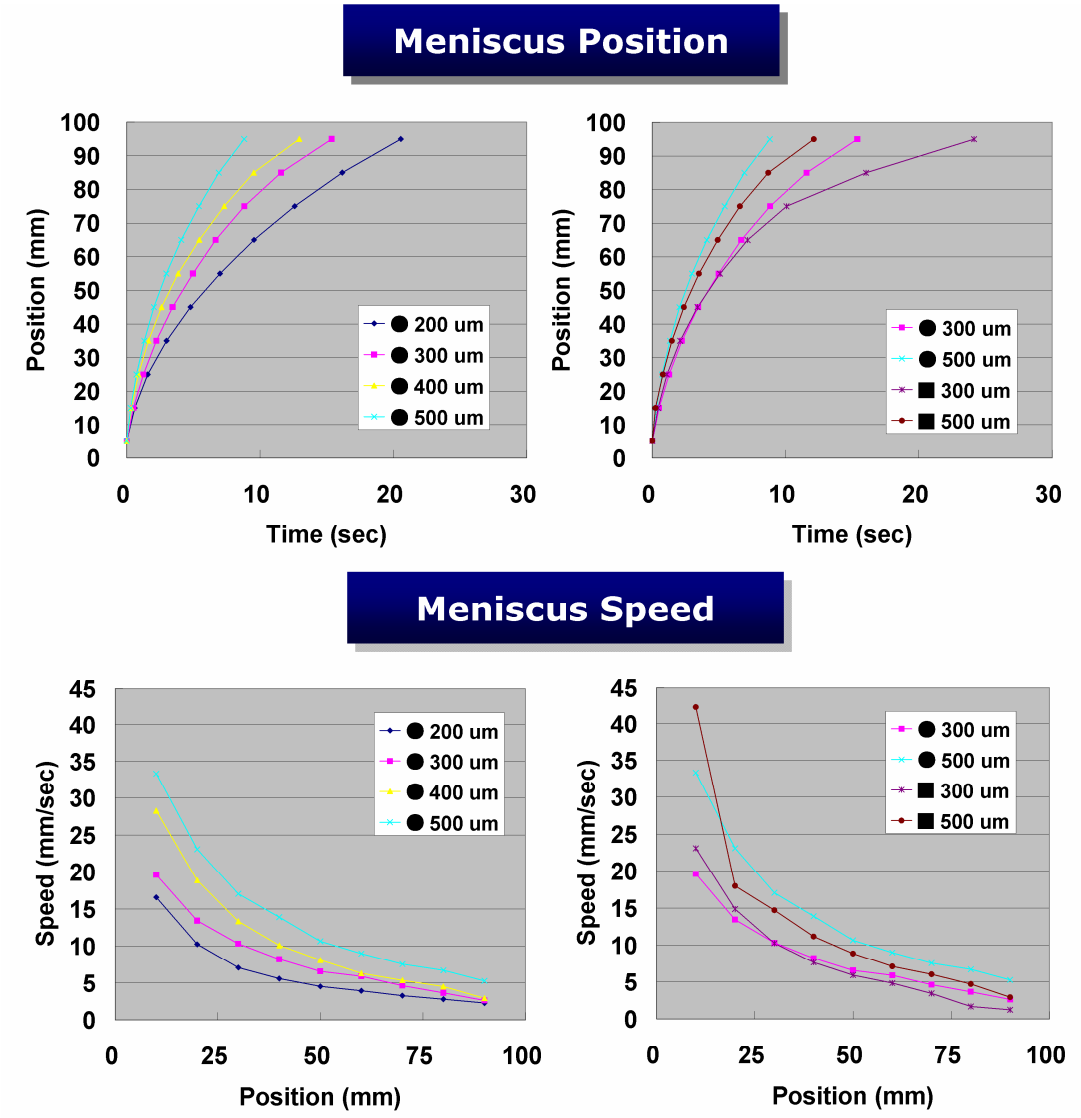

Fig. 2. The meniscus position over time for the different microchannels was obtained by video analysis, and meniscus speed was computed for each position. Elapsed time for the meniscus to reach a position was obtained by averaging three ensemble sets. Three circular microchannels with inner diameters of 300, 400, and 500 μm and two square microchannels with widths of 300 and 500 μm were used and are indicated by symbols in the legends.

where h is the meniscus position from the inlet of the microchannel, a is the inner radius of the microchannel, Γ is the surface tension, θ is the contact angle, μ is the apparent viscosity, and t is the time. The meniscus speed in the square microchannel was faster than in the circular counterpart in the beginning but slowed later as shown in Fig. 2. In the beginning, the surface tension force prevailed and the flow in the square microchannel driven by a bigger surface tension had a higher meniscus speed. While blood was wetting the microchannels, the friction force came into play. The friction force in the square channel was 1.125 times greater if the meniscus speed was the same as that of the circular microchannel. The flow, therefore, in the square microchannel decelerated quickly, and the meniscus speed eventually became slower.

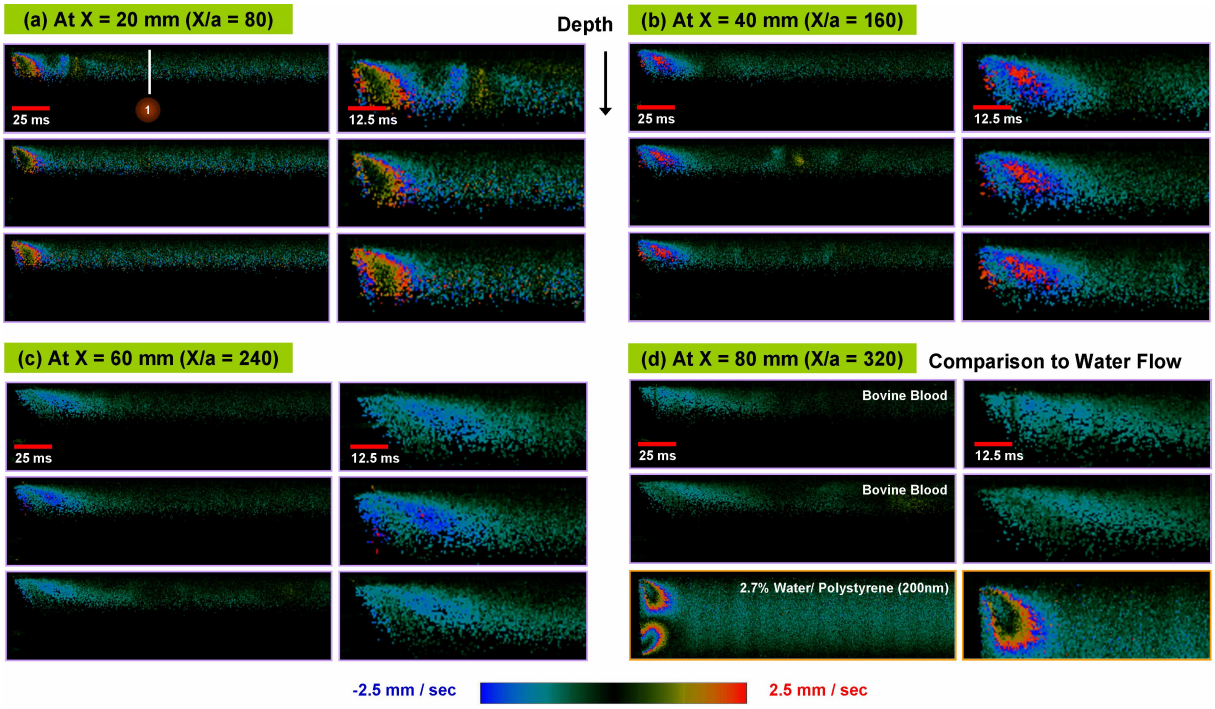

Fig. 3. The radial velocity imaged by SDDOCT is shown. All cases are for the circular microchannel with an inner diameter of 500 μm. The images are depth versus time plots at different fixed positions (X = 20, 40, 60, and 80 mm) which mean the time histories of the radial velocity along the diameter of the microchannel. Here, X is the distance from the inlet of the microchannel. The time history was taken three times for each position corresponding to three rows in Fig. 3(a)-(d). (Only two of three are shown in Fig. 3d.) The second column in Fig. 3(a)-(d) shows enlarged upper half images. The left side of each image indicates the time when menisci reached the probe beam of SDDOCT. The radial blood flow pattern is compared to the radial water flow pattern in Fig. 3(d).

The radial velocity imaged by SDDOCT is shown in Fig. 3. All cases are for the circular microchannel with an inner diameter of 500 μm. The images in Fig. 3 are depth versus time plots at different fixed positions (X = 20, 40, 60, and 80 mm) which mean the time histories of the radial velocity along the diameter of the microchannel. Here, X is the distance from the inlet of the microchannel. The time history was taken three times for each position corresponding to three rows in Fig. 3(a)-(d). (Only two of three are shown in Fig. 3d.) Blood has strong light scattering because of the difference of refractive indices between erythrocytes and plasma and a strong absorption by hemoglobin. Hence, light penetration depth into the blood was limited to 300 μm out of a 500 μm inner diameter. By considering an axisymmetric flow pattern, we show enlarged upper half images in the second column in Fig. 3(a)-(d). The left side of each image indicates the time when menisci reached the probe beam of SDDOCT. The radial velocity was mapped in the color shown in the color map at the bottom of Fig. 3. Each image has an elliptic color pattern. The outermost color in the pattern indicates the direction of the radial velocity. The outermost color of all images in Fig. 3 is blue which means that the direction of the radial velocity is upward (negative). The red color at the center of the elliptic pattern, for instance, in Fig. 3(b) does not mean positive velocity but is more negative because there is an abrupt color change from blue to red. A strong negative velocity caused an aliasing effect or a phase wrapping.[16] The strong radial velocity toward the wall implies that the axial blood velocity at the center of the microchannel is faster than the meniscus speed in order to satisfy the equation of continuity. If an observer follows the moving meniscus, he will observe a clockwise recirculation near

meniscus. Remembering the flow is axisymmetric, we can infer the recirculation from the core of the circular microchannel to the wall along the interface between blood and gas. The decreasing tendency of the radial velocity against the probe beam position was almost the same as that of the meniscus speed. Additionally, we compared the radial blood flow pattern against the radial water flow pattern in Fig. 3(d). We used neutrally buoyant polystyrene beads with a mean diameter of 200 nm as seeding particles in a water experiment. Because of low absorption by the water, we could see the entire cross section along the channel diameter. Surface tension of blood is half water, and viscosity is 4 times greater than water. The meniscus speed in the water experiment was much faster and as was the radial velocity.

The difference of the meniscus speed and the maximum axial blood velocity at the center of the microchannel in the downstream far enough not to have any radial velocity is a measure of strength of the radial velocity at a certain time. We measured the axial velocity profile of blood flow at $X = 20$ mm at three different times (0.09, 1.23, and 2.38 seconds later after the meniscus reached the probe beam located at $X = 20$ mm) and plotted them in Fig. 4. In the downstream far enough not to have any radial velocity, the velocity has only an axial component and, therefore, the Doppler angle is easily determined if we consider the 2^{o} tilted angle of the microchannel. Then, the axial blood velocity can be obtained from the Doppler shift measured by SDDOCT. The number 1 indicated in Fig. 3(a) corresponds to 0.09 seconds. The axial blood velocity decreased with time. Assuming the profile follows Poiseuille's law, we provided parabolic curve fits with the same flow rates (calculated from the experimental data) for three cases. Maximum velocities were 29.4, 22.9, and 19.5 mm/sec, respectively. Since the meniscus speed is almost constant (23 mm/sec from Fig. 2) during such a short time of 0.09 seconds, the measure of strength of the radial velocity was 6.4 mm/sec, and it was 28% of the meniscus speed.

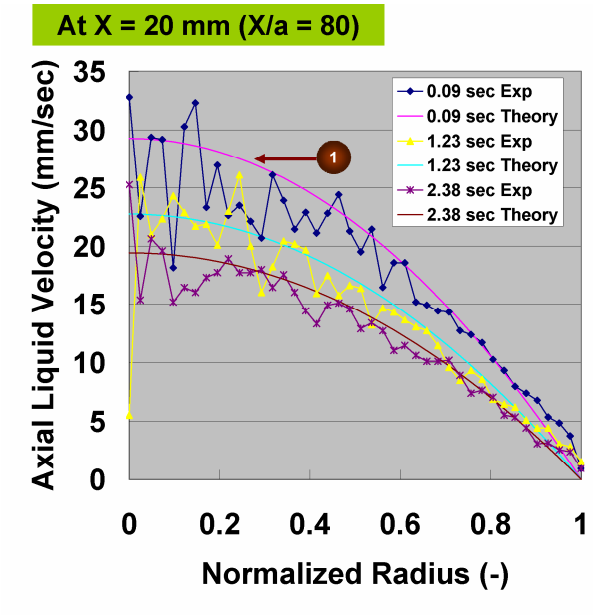

Fig. 4. In the downstream far enough not to have any radial velocity, the axial velocity profile of blood flow at $X = 20$ mm was measured at three different times (0.09, 1.23, and 2.38 seconds later after the meniscus reached the probe beam located at $X = 20$ mm). By assuming that the profile follows Poiseuille's law, parabolic curve fits were provided with the same flow rates calculated from the experimental data.

4. CONCLUSIONS

In this study, we measured and analyzed the surface-tension-driven blood flow with spectral-domain Doppler optical coherence tomography (SDDOCT) and a video camera. From the video analysis, we obtained the meniscus position over time for different shaped microchannels and computed the meniscus speed for each position. Three-dimensional flow

field around the meniscus was quantified by SDDOCT. The radial motion near the meniscus was clearly observed which is a key mechanism to enhance mass transfer from or to the channel wall.

5. ACKNOWLEDGMENTS

The authors acknowledge the support of the National Institutes of Health (EB-00293, NCI-91717, RR-01192), and the Air Force Office of Scientific Research (FA9550-04-1-0101). Institutional support from the Beckman Laser Institute Endowment is also gratefully acknowledged. In addition, the authors acknowledge the international financial supports from the Commission of the European Communities specific RTD IST-2002-1-001837 HEALTHY AIMS, the BE/2006 AGAUR fellowship from the Generalitat de Catalunya, Spain, and the California Catalunia Engineering program. The authors thank the support from Dr. Rodrigo Martinez and Prof. Marc Madou.

REFERENCES

[1] R. Lucas, "Ueber das Zeitgesetz des kapillaren aufstiegs von flüssigkeiten," Kolloidn. Zh. **23**, 15-22 (1918).
[2] E. W. Washburn, "The dynamics of capillary flow," Phys. Rev. **17**, 273-283 (1921).
[3] P. G. deGennes, "Wetting: static and dynamic," Rev. Mod. Phys. **57,** 827–863 (1985).
[4] E. B. Dussan, "On the spreading of liquids on solid surfaces: static and dynamic contact angles," Annu. Rev. Fluid Mech. **11**, 371–400 (1979).
[5] I. Veretennikov, A. Indeikina, and H. C. Chang, "Front dynamics and fingering of a driven contact line," J. Fluid Mech. **373**, 81–110 (1998).
[6] C. Clanet and D. Quéré, "Onset of menisci," J. Fluid Mech. **460**, 131–149 (2002).
[7] S. Basu, K. Nandarumar, and J. H. Masliyah, "A study of oil displacement on model surfaces," J. Colloid Interface Sci. **182**, 82–94 (1996).
[8] P. van Remoortere and P. Joos, "About the kinetics of partial wetting," J. Colloid Interface Sci. **160**, 387–96 (1993).
[9] N. Ichikawa and Y. Satoda, "Interface dynamics of capillary flow in a tube under negligible gravity condition," J. Colloid Interface Sci. **162**, 350–355 (1994).
[10] M. M. Weislogel, "Steady spontaneous capillary flow in partially coated tubes," AIChE J. **43**, 645–654 (1997).
[11] A. Hamraoui, K Thuresson, T. Nylander, and V. Yaminsky, "Can a dynamic contact angle be understood in terms of a friction coefficient?," J. Colloid Interface Sci. **226**, 199–204 (2000).
[12] W. Huang, R. S. Bhullar, and Y. C. Fung, "The surfacetension-driven flow of blood from a droplet into a capillary tube," Trans. ASME J. Biomech. Eng. **123**, 446–454 (2001).
[13] L. J. Yang, T. J. Yao, and Y. C. Tai, "The marching velocity of the capillary meniscus in a microchannel," J. Micromech. Microeng. **14**, 220–225 (2004).
[14] W. K. Chan and C. Yang, "Surface-tension-driven liquid-liquid displacement in a capillary," J. Micromech. Microeng. **15**, 1722–1728 (2005).
[15] S. Chakraborty, "Dynamics of capillary flow of blood into a microfluidic channel," Lab Chip **5**, 421-430 (2005).
[16] Y.-C. Ahn, W. Jung, and Z. Chen, "Optical sectioning for microfluidics: secondary flow and mixing in a meandering microchannel," Lab Chip **8**, 125-133 (2008).